AIAA JOURNAL
Vol. 45, No. 11, November 2007

Evaluation of Precracking Methods for the End-Notched Flexure Test

Carlos L. Perez* and Barry D. Davidson†
Syracuse University, Syracuse, New York 13244

DOI: 10.2514/1.24188

Results are presented from a study to evaluate and develop static mode-II precracking methods for use with the end-notched flexure test. Precracking followed by fracture toughness testing was performed on specimens from two different materials. Precracking was performed using both the four-point-bend and conventional three-point-bend end-notched flexure geometries. All testing was performed in the latter geometry. There was no difference in the precracks created by the two geometries. However, delamination toughness was observed to strongly depend on the amount of dynamic crack advance that occurs during the precracking process. This was hypothesized to be due to the faster crack speeds that are associated with larger amounts of advance. To address this, various precracking geometries were evaluated to determine those that would produce precracks that were essentially straight, perpendicular to the direction of crack advance, and of sufficient length to produce a precracked toughness at or near the minimum value that occurs with increasing precrack length. This results in a recommended geometry for use with the end-notched flexure test that is appropriate for both precracking and testing, and which therefore allows for nonprecracked and precracked toughnesses to be obtained from the same test specimen.

Introduction

BASED on a series of recent studies [1–3], the American Society for Testing and Materials (ASTM) committee D30 on composite materials has resolved to adopt the end-notched flexure (ENF) test as the standard method for determining the mode-II delamination toughness G_{IIc} of laminated composites. Based on the work of [4], ASTM committee D30 has agreed that the new test standard should specify that precracking (PC) of ENF specimens is required. There was consensus that mode-II static precracks should be specified, if possible, because it is expected that these will produce the most accurate values of G_{IIc} [5–8]. However, there is insufficient data in the literature to indicate a preferred mode-II static precracking method that produces a toughness that is both accurate and repeatable. Thus, additional study was required to resolve this issue before a test standard could be prepared for balloting.

The present work describes an investigation designed to resolve the preceding issue. The first part of this study (phase I) evaluated the method of precracking. Here, it was examined whether using the four-point-bend end-notched flexure (4ENF) test to create precracks had any advantages compared with creating precracks in the ENF fixture. This was considered because delamination growth is stable in the 4ENF test [9], and experimental results from the 4ENF [9–11] have indicated that the shape of the delamination after propagation may be straighter than that typically observed when creating mode-II precracks using the ENF [4,5,12–14]. As part of the phase-I investigation, it was observed that G_{IIc} was a function of the amount of crack advance that occurred during precracking. Thus, phase II of the study examined this issue in greater depth to determine whether or not this effect was real and, if so, what caused it and what its ramifications were with respect to developing a static mode-II precracking method for use with the ENF test.

Presented as Paper 1667 at the 47th AIAA/ASME/ASCE/AHS/ASC Structures, Structural Dynamics, and Materials Conference, Newport, RI, 1–4 May 2006; received 24 March 2006; revision received 19 February 2007; accepted for publication 11 March 2007.

*Undergraduate Student, Department of Mechanical and Aerospace Engineering. Student Member AIAA.

†Laura J. and L. Douglas Meredith Professor, Department of Mechanical and Aerospace Engineering. Associate Fellow AIAA.

Materials, Fixtures, and Geometries

Materials and Specimens

All tests conducted as part of this study were on 24- and 32-ply unidirectional IM7/8551-7 and T800H/3900-2 graphite/epoxy specimens. Both of these materials have relatively high toughnesses. In the former material, this is achieved through the use of rubber particles in the matrix [6], and in the latter, it is achieved through the use of thermoplastic particles in the interlayer regions between plies [15]. All specimens were fabricated at the Syracuse University Composite Materials Laboratory following the manufacturer's recommended procedures. Two plates were manufactured of each thickness of the IM7/8551-7 material (subsequently referred to as IM7) and, to allow for the possibility of plate-to-plate variation, the plate number from which the data were obtained will be identified in subsequent results. Two 24-ply T800H/3900-2 (subsequently referred to as T800H) plates were also manufactured, but only one plate was used for all of the results presented herein. Only a single 32-ply T800H plate was manufactured. During layup, two 13-μm-thick Teflon inserts were placed at the midplane of each plate: one at each longitudinal end. Each insert went across the plate's full width (in the 90-deg direction) and extended inward 63.5 mm (in the 0-deg direction) from each free end toward the plate's interior. Following manufacture, the longitudinal ends of the plates were trimmed and the remaining portions were cut into specimens with a nominal width of 22 mm. Silver spray paint was applied to the edges of the specimens to aid in subsequent marking and in the visual identification of crack advance. Each specimen was then ultrasonically inspected (C-scanned) to identify the endpoint of its insert. This location was then marked on both painted edges using a fine-point mechanical pencil. In most instances, both ends of the specimen were tested. Here, it was always verified that the cracked end that was not being tested did not enter into the region of the specimen that was subjected to bending stress.

Fixture Design

As described earlier, both the ENF and 4ENF test fixtures, shown schematically in Fig. 1, were used as part of this study. Notice that the only real difference between these two fixtures is in the upper loading head. Considering the similarities, and because the 4ENF geometry was used solely for creating precracks, it was desired to have a test

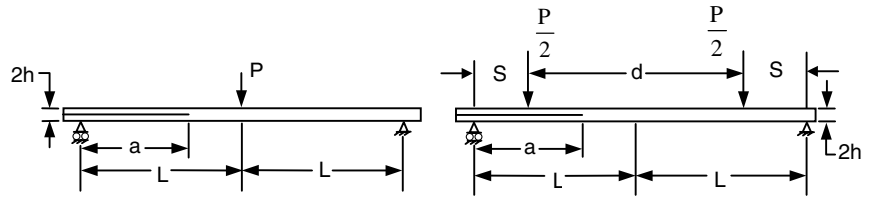

a) b)

Fig. 1 Schematic representations of a) ENF and b) 4ENF tests.

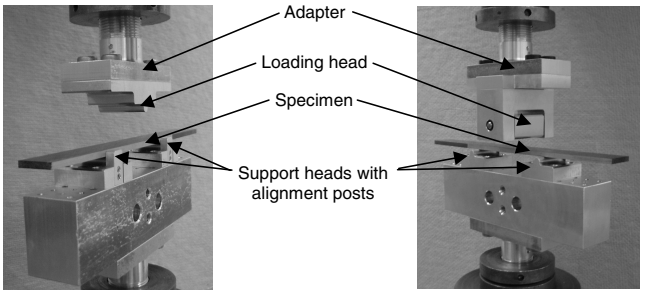

a) b)

Fig. 2 Photographs of a) ENF and b) 4ENF fixtures.

fixture that could rapidly be changed from one configuration to the other. As shown in [1,3], a stiff fixture is also necessary to obtain accurate toughness values, and so fixture stiffness was also a driver of design.

The resulting fixture design is shown in Fig. 2. All components are made from aluminum. The relatively rigid lower platen allows values of $2L$ (cf. Fig. 1) to be used from 38.1–177.8 mm in 12.7-mm increments. As shown in the figure, the two support heads sit on the lower platen. They are essentially T-shaped pieces that are 31.8 mm wide with a machined head diameter of 6.35 mm. They also have a machined vertical line down their center that coincides with the center point of the loading head and that can be used to align marks made on the specimen to obtain the desired crack length. Attached to each support head is an alignment post against which the specimen is placed to ensure that it is longitudinally aligned with the fixture. With the exception of the alignment posts, the ENF loading head is identical to the support heads. The loading head for the 4ENF fixture uses a clevis arrangement to allow free rotation [9–11]. The inner portion of the clevis consists of a single piece with two integrally machined 6.35-mm-diam loading heads, where the distance d between contact points is 38.1 mm (cf. Fig. 1). As shown in Fig. 2, the ENF and 4ENF loading heads attach to a common adapter that attaches to the load frame.

To align the fixture, the upper loading head is brought close to the lower platen and rigid alignment jigs are attached on each side of the lower platen. This is achieved using the four holes that are visible on the side of the platen in Fig. 2. Two of these holes are for bolts and two are for alignment dowels. This alignment jig holds the lower platen and upper adapter parallel while all the collars that attach the fixture to the load frame are tightened. Thereafter, the alignment jig is removed and the loading head can be interchanged from ENF to 4ENF using only the four bolts that attach it to the adapter.

Test and Precracking Geometries

In what follows, the term *test geometries* is used to denote those configurations that were tested to obtain $G_{\mathrm{II}c}$, whereas *precracking geometries* is used to denote those configurations that were used to advance the delamination front and create a precrack. In both instances, *geometries* refers to the choice of specimen thickness, crack length, and span length. Initially, test geometries for this study were chosen following the guidelines described in [16,17]. These guidelines aim to ensure that 1) the compression stress from the central loading head does not affect the critical energy release rate, 2) the expression used for compliance calibration (described subsequently) is valid for the range of crack lengths in which it is applied, and 3) geometric nonlinear behaviors do not affect the toughness as obtained by the compliance calibration method of data reduction. Near the midpoint of the current study, [18] became available, which included a comprehensive study of test geometries and data reduction procedures, but only for cases in which the crack was equal to 50% of the half-span length ($a/L = 0.5$). Because the test geometries chosen by the method of [16,17] were for $a/L \approx 0.6$, two new test geometries were added to ensure that these former geometries produced the same value of $G_{\mathrm{II}c}$ as those chosen by the method of [18].

When creating precracks using the 4ENF, all specimens used $a = L$ (cf. Fig. 1b). All 24-ply specimens (i.e., both materials) used a span length of $2L = 88.9$ mm, and all 32-ply specimens used $2L = 101.6$ mm. As indicated previously, d was always equal to 38.1 mm. Based on the results of [4,5,12–14], $a/L \approx 0.9$ was initially chosen for creating precracks using the ENF for the phase-I study. However, in an attempt to obtain precracks of various shapes, a few specimens were also precracked in the ENF at $a/L \approx 0.6$ during phase I. During phase II, values of a/L equal to 0.50 and approximately 0.73 were also considered.

A summary of the ENF geometries used for both precracking and testing is presented in Table 1. The first column of this table presents the laminate and phase of the study. Here and subsequently, I24 and I32 refer to the 24- and 32-ply IM7 specimens, respectively, −1 and −2 refer to the two different plates that were manufactured, and −I and −II refer to the phase-I and phase-II studies, respectively. Similarly, T24 and T32 are used for the 24- and 32-ply T800H specimens, respectively. Here, no plate number is indicated, because all specimens of each thickness came from the same plate. The second column of Table 1 provides designations for the geometries used for these tests, the third and fourth columns indicate which geometries were used for PC and which were for testing, and the final three columns provide the associated test geometries. It can be observed from this table that all phase-I tests on the IM7 material were performed using I24-1 and I32-1 specimens. Further, the majority of

Table 1 ENF geometries used for precracking and testing

Laminate and phase	Geometry	PC	Test	a, mm	$2L$, mm	a/L
I24-1-I	I24A	x		38.10	88.90	0.86
I24-1-I, I24-1-II, I24-2-II	I24B	x	x	26.67	88.90	0.60
I24-1-II, I24-2-II	I24C	x	x[a]	28.58	114.3	0.50
I24-2-II	I24D	x		33.02	88.90	0.74
I32-1-I	I32A	x		50.80	114.3	0.89
I32-1-I, I32-1-II, I32-2-II	132B	x	x	33.02	114.3	0.58
I32-1-II, I32-2-II	I32C	x	x[b]	38.10	152.4	0.50
I32-2-II	I32D	x		41.91	114.3	0.73
T24-I	T24A	x		38.10	88.90	0.86
T24-I, T24-II	T24B	x[c]	x	26.67	88.90	0.60
T32-I	T32A	x		50.80	114.3	0.89
T32-I, T32-II	T32B	x[c]	x	33.02	114.3	0.58

[a]Tests in this configuration were only performed on nonprecracked specimens and on four precracked CWS specimens.
[b]Tests in this configuration were only performed on nonprecracked specimens and on two precracked CWS specimens.
[c]Precracking in this configuration was only performed during phase II.

the precracks during phase I were created using geometries I24A and I32A; only a few specimens were precracked during this phase using geometries I24B and I32B. As indicated in Table 1, all phase-I IM7 tests were performed using geometries I24B and I32B. For the T800H material, all precracks during phase I were created using geometries T24A and T32A, and all of these specimens were tested using geometries T24B and T32B. The average thicknesses of the specimens from plates I24-1, I24-2, I32-1, and I32-2 were 3.43, 3.45, 4.57, and 4.54 mm, respectively, and the average thicknesses of the T24 and T32 specimens were 4.40 and 5.89 mm, respectively.

As indicated in Table 1, the largest values of a/L were used only in the phase-I study. Work during phase II concentrated on creating precracks using test geometries in the range of $0.50 \leq a/L \leq 0.74$. Referring to the table's footnotes, CWS indicates "curved, wavy, or slanted" precracks (i.e., precracks that were not straight and perpendicular to the direction of crack advance). Thus, as indicated by footnotes a and b, no tests on precracked specimens with straight delamination fronts were performed using geometries I24C and I32C. Rather, these geometries were primarily used for 1) creating precracks and 2) testing nonprecracked (NPC) specimens (i.e., directly from the Teflon insert). The latter tests were performed and the results were compared with those from tests in the nonprecracked I24B and I32B configurations. As previously described, this was done because the I24B and I32B geometries were chosen by the method of [16,17], whereas test configurations I24C and I32C are within the range recommended by [18]. Therefore, the nonprecracked tests were used to verify that these two test geometries produced equivalent results (i.e., to ensure that the choice of test geometry did not influence the overall conclusions). Nonprecracked, rather than precracked, specimens were used for this substudy to eliminate any influence of precrack shape on the results. In the interest of brevity, and because these results are not of direct importance to the present study, we state here that statistically identical results were obtained by the different test geometries, and the geometries used herein are therefore expected to produce highly accurate toughness values. Complete results of this portion of the study are presented in [8].

Precracking, Inspection, Testing, and Data Reduction

Precracking and Nondestructive Inspection Procedures

All precracking and testing was performed in an MTS servo-hydraulic load frame under displacement controlled loading at a rate of 0.0127 mm/s, and all load and displacement data was plotted in real time and saved for later data manipulation. For those specimens precracked using the 4ENF, a few trial tests indicated that the load versus displacement (P-δ) results agreed with those typically reported in the literature [9–11]: the curve became nonlinear around the time of crack advance and remained at a near-zero slope as the crack continued advancing. Thus, when precracking using the 4ENF, loading was stopped when the P-δ curve showed the distinct nonlinearity that is associated with delamination growth. The amount of crack advance that occurred during 4ENF precracking, defined here as Δa, varied from specimen to specimen as a result of 1) the difference between the initiation and the propagation toughness and, to a certain extent, 2) the amount of time that elapsed from when the nonlinearity occurred until the test was stopped. The former effect was by far the more dominant for the IM7 specimens. That is, in these specimens, crack growth during precracking can be interpreted primarily as dynamic unstable advance over the length Δa. This is consistent with the large difference between the nonprecracked and precracked toughness that has been reported for this material [6] and that was observed in this work. The latter effect dominated for 4ENF precracking of the T800H material and is consistent with the precracked toughness being equal to or slightly greater than the nonprecracked value for this material [11].

As would be expected, a nonlinear region before crack advance was also observed when precracking using the ENF and high values of a/L (0.86 and 0.89). Here, crack speeds were relatively low, and the specimen was unloaded when the nonlinearity was observed. Subsequent C-scans indicated that this corresponded to delamination growth to the center loading head. However, in one early specimen, the precracking test was run a bit longer before being stopped, and it was found that the delamination grew slightly beyond this point. In contrast, when the ENF was used with $0.5 \leq a/L \leq 0.6$, crack growth was very rapid, unstable, and was associated with a large load drop. Subsequent C-scans indicated that these delaminations also grew to the center loading head. For $a/L = 0.73$ or 0.74, growth during precracking was similar to that observed in the 4ENF. Here, the crack grew at a rate that appeared to be between that observed for $a/L = 0.6$ and $a/L = 0.9$. Thus, the net result of all these different ENF precracking geometries is that the amount of dynamic crack advance that occurred during precracking increased with decreasing a/L. The effect of this on $G_{\mathrm{II}c}$ formed the focus of phase II of this study.

Following precracking, each specimen was C-scanned to determine the shape of its delamination front. All scans were performed using a 10-MHz transducer in pulse-echo mode connected to a 100-MHz transient waveform digitizer to collect and relay these data to a personal computer for storage. Both amplitude and time-of-flight data were taken, but based on previous studies [19–21], the time-of-flight data was used for assessing delamination-front shapes. All C-scans were performed such that the captured data covered the region of the delamination front to a free end of the specimen. This allowed the crack lengths and the variations in crack length along the delamination front to easily be determined using the nondestructive inspection (NDI) system software. In what follows, toughness values will be plotted versus Δa, the amount of crack advance that occurred during precracking. For this purpose, the new crack length was defined using the equivalent area method, which has been shown to be the most accurate definition for use with the compliance calibration method of data reduction [22]. For crack fronts that are not straight and perpendicular to the specimen's edges, this method defines an area of growth equivalent to that which occurred, but with a straight front normal to the edges, and the location of this front defines the length of the crack. The method was employed using the NDI software to determine the area bounded by the delamination front and the three remaining edges of the specimen and then dividing this area by the specimen's width. This provides the crack length to the end of the specimen, from which the crack length from the insert to the end of the specimen (obtained by an earlier C-scan) was subtracted. Finally, subsequent to precracking but before C-scanning, the crack length for some specimens was determined visually from the specimen's edges. This was performed both under load and not under load, for later comparison with the C-scan measurements.

Subsequent to all testing, the accuracy of the C-scan images was assessed by performing posttest scans of three different specimens, splitting these specimens open in mode I, and, for each specimen, measuring the marks left at the end of the mode-II crack at five different locations across the width. The visually observed shapes agreed quite well with the C-scan images, with the exception that the visually apparent delamination-front marks formed a smoother curve. That is, local peaks and valleys that appeared in the C-scans were not evident. Rather, the visually observed delamination front appeared to follow a path that averaged the locally sharp peaks and valleys of the C-scan images. It was found that the 15 different physical measurements agreed with those made by the C-scan software within an average of 1.2%. Considering this and the results obtained by a similar comparison using destructive sectioning [21], it was concluded that the C-scanned shapes were highly accurate.

Testing and Data Reduction

The compliance calibration (CC) method was used to obtain delamination toughnesses from all tests that were conducted. This method uses the relation [1,3,9–12,16–19]

$$G_{\mathrm{II}c} = \frac{P_c^2}{2B}\left[\frac{\partial C}{\partial a}\right]_{a=a_c} \tag{1}$$

where P_c is the load at the onset of delamination growth, C is the specimen's compliance, B is the specimen's width, and a_c is the

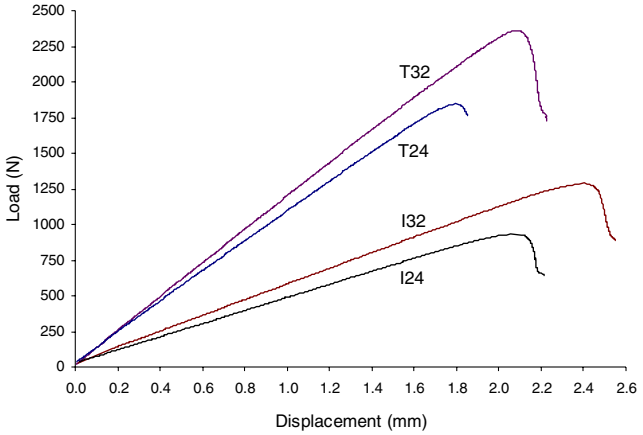

Fig. 3 Typical load versus deflection plots for precracked specimens.

crack length at which the fracture test is performed. To obtain the C versus a relations, each specimen was compliance-calibrated before the fracture test. This was done by shifting the specimen in the ENF fixture to simulate cracks of length a_c, $a_c \pm \Delta$, and $a_c \pm 2\Delta$, where Δ was 5.08 mm for all specimens tested. In accordance with the results and recommendations of [2], at each crack length used for CC, the specimen was loaded to approximately 50% of its critical load, as predicted using classical beam theory for a crack of length $a = a_c$. Thus, at $a = a_c$, the energy release rate during CC was approximately 25% of $G_{\mathrm{II}c}$, whereas it was in the neighborhood of 10% of $G_{\mathrm{II}c}$ at the shortest crack length used during CC and 45% of $G_{\mathrm{II}c}$ at the longest. Following compliance testing, linear fits of the actuator displacement versus load data were used to obtain the compliances at each crack length. These results were fit using the expression [5,18]

$$C = C_0 + C_1 a + C_3 a^3 \tag{2}$$

This expression was shown in [18] to produce values of $G_{\mathrm{II}c}$ that were highly accurate. Following CC, the specimen was placed back into the ENF fixture at $a = a_c$. The specimen was then loaded in displacement control at 0.0127 mm/s until fracture, which was accompanied by a readily observable drop in load. Typical load versus deflection plots are shown in Fig. 3 for precracked specimens of each type. Critical energy release rates were determined from the nonlinear point, the 5% offset/maximum point, and the maximum load point [4,5,13,14,23,24]. That is, the three different definitions of P_c were used when computing $G_{\mathrm{II}c}$ from Eqs. (1) and (2). However, similar to those shown in Fig. 3, all of the load versus deflection plots were essentially linear, and of the 136 tests done in support of this study, the 5% offset/maximum point and the maximum point were identical for all but four of these. Of these four, the two largest differences in $G_{\mathrm{II}c}$ using these definitions of load were only 1.1 and 0.6%. Thus, in what follows, toughnesses are reported based only on the nonlinear and maximum load points.

Phase I: Effect of Precracking Method for IM7/8551-7

Figures 4 and 5 present the key results for IM7/8551-7 from the phase-I study. Figure 4 presents $G_{\mathrm{II}c}^{\max}$ as a function of the amount of advance during precracking, Δa, and Fig. 5 presents analogous results for $G_{\mathrm{II}c}^{\mathrm{NL}}$. In both figures, NPC stands for nonprecracked (i.e., for $G_{\mathrm{II}c}$ as determined directly from the preimplanted Teflon insert). Also, delamination fronts that were essentially straight and perpendicular to the direction of crack advance are indicated by open symbols, and filled symbols are used for other types of delamination fronts. Here and subsequently, a straight precrack is defined as one for which $a_{\max} - a_{\min} \leq 2.8$ mm, where $a_{\max}$ is the maximum point of crack advance anywhere along the delamination front, and $a_{\min}$ is the minimum point. Other types of precracks are referred to as CWS which, as indicated previously, is used for curved, wavy, and/or slanted fronts. This terminology is a carryover from the early portion

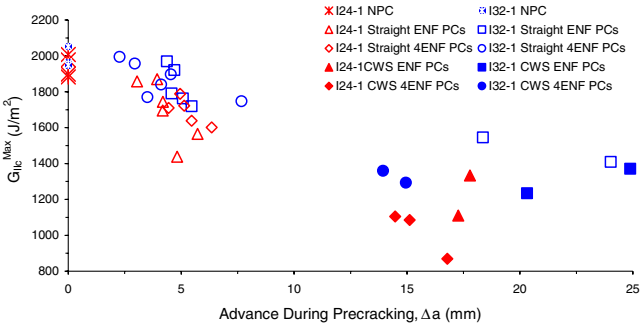

Fig. 4 Effect of precracking method on $G_{\mathrm{II}c}^{\max}$ for IM7/8551-7.

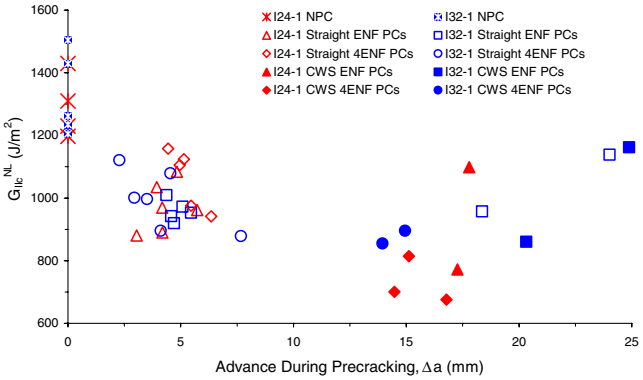

Fig. 5 Effect of precracking method on $G_{\mathrm{II}c}^{\mathrm{NL}}$ for IM7/8551-7.

of this study, in which an effort was made to differentiate between these types of nonstraight fronts. However, as will become apparent subsequently, it was ultimately determined that such differentiation was not required. Thus, CWS is used here simply to refer to those delamination fronts that do not meet the preceding criterion for being straight.

With respect to the straight versus CWS criterion of $a_{\max} - a_{\min} \leq 2.8$ mm, this bounding value was chosen based on a reasonably natural cutoff in the data; that is, there were a large number of specimens with $a_{\max} - a_{\min} \leq 2.8$ mm, but few in which $a_{\max} - a_{\min}$ was just slightly larger. For example, out of all the specimens tested, the next four largest values of $a_{\max} - a_{\min}$ after 2.8 mm were 3.05, 3.18, 3.30, and 3.56 mm. The decision to choose 2.8 mm as the bounding value was based on a subjective visual assessment that these four specimens looked less straight than those with smaller values of $a_{\max} - a_{\min}$. Had the criterion been based on $a_{\max} - a_{\min} \leq 3.5$ mm, it would change the way that three of the preceding four data points are labeled in the figures that present $G_{\mathrm{II}c}$ versus Δa, but it would not change the conclusions that follow. Thus, the value of 2.8 mm is not intended as a universal rule, and any choice between 2.8 and 4.0 mm would not fundamentally change the conclusions that follow.

To illustrate the preceding, typical delamination-front shapes from the IM7 specimens are shown in Fig. 6. The dark portion represents the delaminated region, and the delamination is growing from bottom to top. The top row presents typical specimens that met our criterion for straightness, and the bottom row shows specimens that did not. The center image within the I24 CWS results has $a_{\max} - a_{\min} = 3.68$ mm, and all other I24 and I32 CWS fronts have $a_{\max} - a_{\min} > 4$ mm. The delamination front in the specimen with $a_{\max} - a_{\min} = 3.68$ mm does not appear to be as straight as those in the images in the first row, but classification of this specimen as CWS is certainly somewhat subjective. However, classification of all the other fronts is reasonably straightforward. Thus, the criterion that was adopted produces delamination fronts that essentially appear straight by visual inspection, and this approach would not be affected by a small increase in the cutoff value for $a_{\max} - a_{\min}$.

Referring once again to Figs. 4 and 5, all I24-1 straight ENF PC specimens were precracked using geometry I24A, and all I24-1 CWS

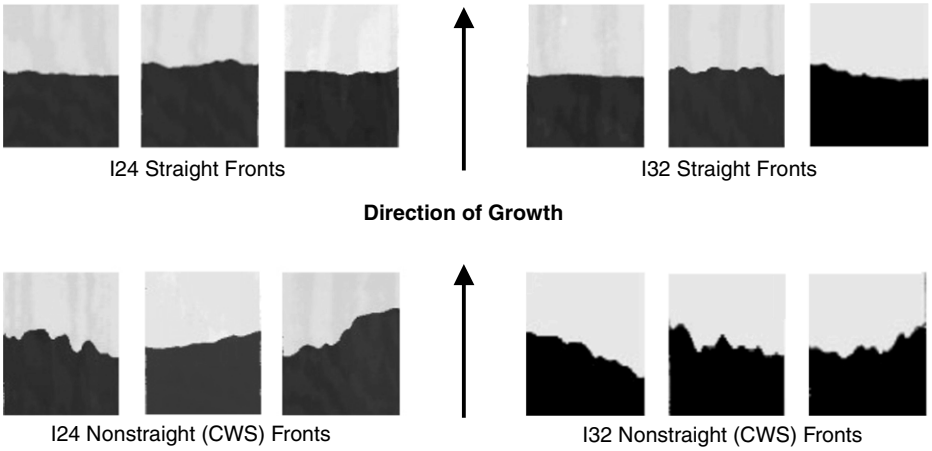

Fig. 6 Typical C-scans from IM7/8551-7 specimens.

ENF PC specimens were precracked using geometry I24B. All I32-1 CWS ENF PC specimens and the two I32-1 ENF PC specimens with large Δa were precracked using geometry I32B; the remaining five specimens in the I32-1 ENF PC set were precracked using I32A. As indicated in Table 1, all I24 specimens were tested using I24B and all I32 specimens were tested using I32B. The NPC data sets from the 24- and 32-ply plates pass the Anderson–Darling pooling test [25], which indicates that these data can be assumed to be from the same population. However, there is perhaps a slight separation of the 24- and 32-ply precracked $G_{\mathrm{II}c}^{\max}$ data sets in Fig. 4. For either thickness, Figs. 4 and 5 indicate that there is no difference between the ENF and 4ENF precracking methods in terms of their propensity for creating straight versus CWS fronts. Rather, it appears that the sole determiner is the amount of crack advance during precracking, with CWS precracks being more likely to occur for larger values of Δa. Specimens with CWS precracks will produce inaccurate values of $G_{\mathrm{II}c}$. This is due to the large variations in the local value of the energy release rate across the specimen's width and the resulting local crack advance that occurs [26], as well as the fact that crack advance from these precracks will not be self-similar [6,7]. Focusing on the results from straight delamination fronts (open symbols) of either thickness, it is clear that there is no effect of the precracking method (ENF versus 4ENF) on the resulting toughness. For specimens with straight crack fronts, it also appears that $G_{\mathrm{II}c}$ decreases with increasing Δa, with the effect being more pronounced for $G_{\mathrm{II}c}^{\max}$ than for $G_{\mathrm{II}c}^{\mathrm{NL}}$.

It is hypothesized that the decrease in $G_{\mathrm{II}c}$ with Δa can be traced to the fact that the magnitude of Δa essentially corresponds to the speed of crack advance during precracking. That is, considering growth from the preimplanted insert, the high nonprecracked toughness shown in Figs. 4 and 5 is a result of the large amount of damage that is created when initiating delamination advance from the relatively blunt insert tip [5,6,13,23,24]. Lesser amounts of this damage are propagated forward with increasing crack speed and distance of growth. Dynamic propagation is also accompanied by a ductile-to-brittle transition in the matrix [27]. Thus, the delamination front from a long dynamically advanced crack will be sharp with minimal near-tip damage and therefore will produce a low value of $G_{\mathrm{II}c}$. Conversely, cracks that are propagated slowly and stably, regardless of the length of crack advance, will "push" the damage zone and there will be little change in the observed value of $G_{\mathrm{II}c}$ [6]. It is therefore important to emphasize that Δa, as used throughout this work, is meant to indicate primarily *dynamic* crack advance that occurs during precracking. We point out that, qualitatively, it appeared that faster crack speeds occurred in the I24-1 than in the I32-1 specimens, which would explain the lower values of $G_{\mathrm{II}c}^{\max}$ in the I24-1 results at any given value of Δa. That is, it is possible that the I24 and I32 $G_{\mathrm{II}c}^{\max}$ results would collapse to a single curve if we were able to accurately measure the speed of the precrack as it grew.

A review of the literature for the effects of crack speed on $G_{\mathrm{II}c}$ was conducted to evaluate the preceding hypothesis. Reference [6] appears to provide results at speeds that are generally below those observed herein and, as such, is not applicable. However, [28] presents data over a range of rates, the upper end of which appears to approach the peak rates that likely occurred herein. Their data indicate a peak in the curve of $G_{\mathrm{II}c}$ versus crack speed at relatively low rates (in comparison with those in this study), with a decrease in $G_{\mathrm{II}c}$ with increasing crack speed thereafter (as the range of rates in this study are approached). This is similar to the effects of crack speed on $G_{\mathrm{I}c}$ in polymers [27]. Reference [28] also examined four other studies on this issue, all of which show $G_{\mathrm{II}c}$ decreasing with crack speed in the vicinity of the rates that likely occurred in the present work. Similar results have been obtained for mode-II fracture of polyurethane adhesive joints [29]. The percentage change with increasing crack speed varies widely among studies, however, and many of the studies have peak rates that are likely lower than those observed here. Also, different results were obtained in [30] on S2/8553 glass/epoxy, in which it was found that $G_{\mathrm{II}c}$ was essentially independent of crack speed. Thus, this issue cannot be fully resolved from the results in the literature, but the majority of the data that are available do appear to support the hypothesis.

From the preceding discussion and the results in Figs. 4–6, it appears that there is no advantage to using the more cumbersome 4ENF precracking method, and precracks should therefore likely be generated within the ENF fixture. They also show that longer precracks will lead to a "minimum toughness," which would be desirable when using the ENF test to develop design properties. However, longer precracks also increase the chances of a CWS front and hence an inaccurate value of $G_{\mathrm{II}c}$. These are competing effects that must be considered when choosing a precracking method. Thus, the focus of phase II of this study was to 1) confirm the preceding and 2) investigate whether a "compromise approach" could be developed for creating precracks within the ENF fixture that would produce relatively straight precracks of sufficient length to be within the minimum toughness regime.

Phase II: Effect of Precrack Length for IM7/8551-7

Figure 7 presents the effect of precrack length on $G_{\mathrm{II}c}^{\max}$ for the 24-ply IM7 specimens. This figure contains all of the 24-ply IM7 data presented in Fig. 4, as well as the new data generated during the phase-II testing (cf. Table 1). However, due to the similarity between toughness results from specimens with ENF and 4ENF precracks, these different precracking methods are no longer distinguished. Thus, the 11 open triangles correspond to the I24-1 straight PC data from Fig. 4, and the five filled triangles correspond to the I24-1 CWS data. The three open squares for which $\Delta a < 5$ mm correspond to specimens precracked in geometry I24A, the two open and one filled square for which 5 mm $< \Delta a <$ 10 mm correspond to specimens precracked in geometry I24D, the open squares in the vicinity of $\Delta a = 16$ mm correspond to those specimens that were precracked in geometry I24B, and the filled squares for which $\Delta a > 25$ mm correspond to specimens precracked using geometry I24C. Results from the I24-1 and I24-2 specimens are differentiated for

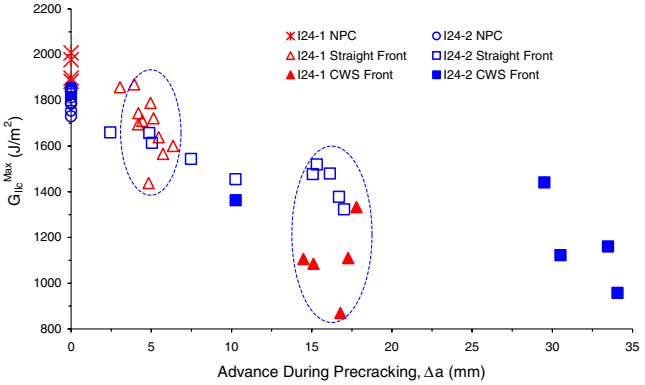

Fig. 7 G_{IIc}^{max} as a function of Δa for 24-ply IM7/8551-7 specimens.

completeness, but based on the results in the figure, these precracked data sets are assumed to belong to the same population. As indicated in Table 1, all of the toughnesses obtained from specimens with straight precracks were generated using test geometry I24B. The data sets enclosed within the dotted ellipses will be discussed subsequently, and these ellipses should be ignored for the purposes of this discussion.

As was observed previously, Fig. 7 shows that G_{IIc}^{max} monotonically decreases with increasing Δa, and that CWS precracks become more likely as Δa increases. For straight precracks, G_{IIc}^{max} appears to approach a limiting value when Δa is in the neighborhood of 16 mm. Interestingly, precracking geometry I24B always produced straight precracks of this approximate length. Geometry I24A also produced straight precracks, but Δa was too short to be in the minimum-toughness regime. Geometry I24D sometimes produced straight precracks and sometimes produced CWS fronts, and geometry I24C always produced CWS results.

Figure 7 also shows that as long as one considers only straight precracks, then the scatter in G_{IIc}^{max} does not increase with increasing Δa. However, if all data are included, then this is no longer the case. This is better illustrated in Fig. 8. Here, the discrete data points plot the mean value of selected data sets and the error bars present the associated ± 1 normal standard deviations. The results in Fig. 8 at $\Delta a = 0$ correspond to all of the nonprecracked data of Fig. 7, and the results at $\Delta a = 4.9$ mm are obtained from the data shown in the dotted ellipse centered at this value of Δa in Fig. 7. This data set and the other set within an ellipse in Fig. 7 were chosen because they appeared to be at sufficiently close values of Δa to allow meaningful averages and standard deviations to be computed. The open symbol in Fig. 8 at $\Delta a \approx 16$ mm corresponds to the results from the open symbols within the corresponding ellipse in Fig. 7 (i.e., the mean and standard deviation data from all specimens precracked using geometry I24B). Similarly, the results at this value of Δa in Fig. 8 for all precracked data and for CWS precracks only come from the corresponding data sets within the associated ellipse of Fig. 7. From Fig. 8, it is clear that the dispersion of data does not increase with Δa provided that one can obtain only straight precracks. Thus, if a method of developing straight precracks with large Δa is developed,

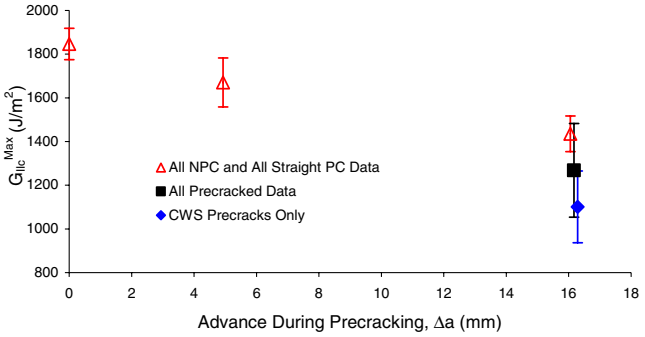

Fig. 8 Mean and standard deviation in G_{IIc}^{max} of selected 24-ply IM7/8551-7 data sets as a function of Δa.

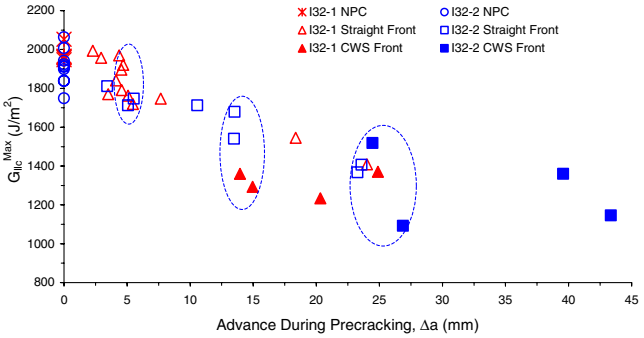

Fig. 9 G_{IIc}^{max} as a function of Δa for 32-ply IM7/8551-7 specimens.

these results indicate that there will be no difference in the reproducibility of the associated toughness values compared with toughnesses generated from shorter precracks. It therefore follows that minimum-toughness values obtained from specimens with long straight precracks should not suffer from any greater scatter than toughness values obtained from specimens with shorter precracks.

Figure 9 presents results for the I32 specimens that are analogous to those presented in Fig. 7. The I32-1 results are the same as those presented in Fig. 4. The three open squares for which $\Delta a < 6$ mm are from specimens precracked in geometry I32A, and the three for which 10 mm $< \Delta a <$ 15 mm correspond to specimens precracked in geometry I32D. The four squares contained in the ellipse at $\Delta a \approx 25$ mm were precracked in geometry I32B, and the two filled squares at large Δa were precracked in geometry I32C. As in the preceding results, this figure shows that G_{IIc}^{max} for straight precracks monotonically decreases with increasing Δa. Here, the minimum toughness occurs in the vicinity of $\Delta a = 25$ mm, compared with $\Delta a \approx 16$ mm in the I24 specimens. However, note that the minimum-toughness values that are observed in Figs. 7 and 9 for specimens with straight delamination fronts are essentially the same. This lends credibility to the hypothesis that it is crack speed during precracking, and not the actual value of Δa, that is responsible for the decrease in G_{IIc}. It is also of interest and importance to note that, similar to the I24 results, those specimens precracked in the I32C geometry never exhibited straight delamination fronts. However, unlike the I24 results, the I32B precracking geometry sometimes produced straight delamination fronts, but often did not. Thus, a comparison with the I24 results indicates that it is not only the value of a/L that is important in creating straight precracks, but the magnitude of $L - a$ as well. Larger values of $L - a$ mean that the crack will travel longer distances before being arrested by the center roller. This increases the probability of obtaining a CWS front.

Figure 10 presents results that are analogous to those of Fig. 8, but for the I32 specimens. Here, the mean and normal standard deviation results from the nonprecracked data, as well as the data enclosed in the three ellipses of Fig. 9, are plotted versus Δa. However, because the ellipses at $\Delta a \approx 14$ and 25 mm have limited amounts of data, meaningful averages and standard deviations cannot be computed for the CWS and straight precrack data sets separately. For this

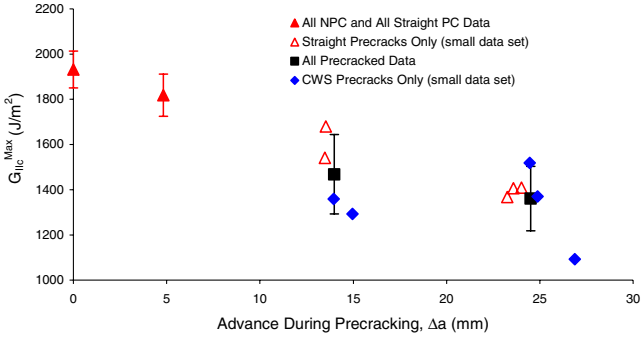

Fig. 10 Mean and standard deviation in G_{IIc}^{max} of selected 32-ply IM7/8551-7 data sets as a function of Δa.

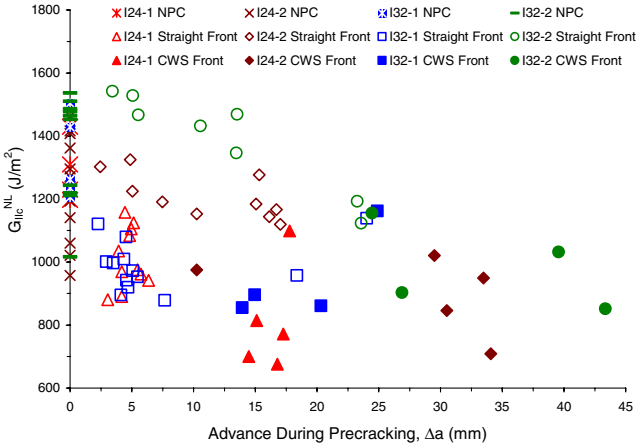

Fig. 11 G_{IIc}^{NL} as a function of Δa for IM7/8551-7.

reason, the mean and standard deviations are presented for the combined data, but discrete data points are presented for the straight and CWS results. Figure 10 indicates that the same conclusion holds true for the I32 as for the I24 specimens: considering only straight delamination fronts, there is no significant increase in scatter with increasing Δa.

Figure 11 presents G_{IIc}^{NL} as a function of crack advance for all of the IM7 specimens tested. Similar to the comparisons in Figs. 4 and 5, G_{IIc}^{NL} is observed to decrease with increasing Δa, but the effect is not as pronounced as that observed for G_{IIc}^{max}. It is also interesting to note that the data from a given thickness plate do not pool well. This agrees with the results in [6], which indicate that the nonprecracked value of G_{IIc}^{NL} will be geometry-dependent. As such, it is not clear that G_{IIc}^{NL} has any physical meaning, and current plans are to *not* require reporting of this value in the ENF standard [8]. Nevertheless, these are included here and subsequently for completeness.

Phases I and II Results for T800H/3900-2

Figures 12–14 present results for the T800H material. Figures 12 and 13 present G_{IIc}^{max} and G_{IIc}^{NL} data, respectively, for all T800H specimens that were tested as part of this study, and Fig. 14 presents typical delamination-front shapes for specimens precracked in the ENF and 4ENF fixtures. From Figs. 12 and 13, it is clear that the amount of testing performed on T800H was not as extensive as that done using IM7. This was because the precracking methods examined always produced straight delamination fronts in this material. This may be observed from the images in Fig. 14. As a result, the T800H data did not prove to be as rich of a source of information in terms of the overall goals of this study.

Referring once again to Fig. 12, it may be observed that there is no effect of precracking method (ENF versus 4ENF) on G_{IIc}^{max}. Also, for

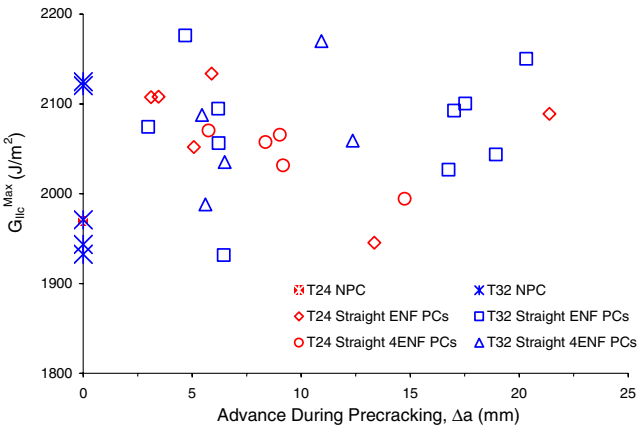

Fig. 12 G_{IIc}^{max} as a function of precracking method and Δa for T800H/3900-2.

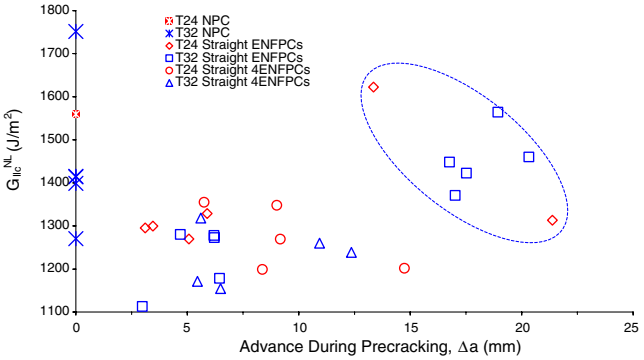

Fig. 13 G_{IIc}^{NL} as a function of precracking method and Δa for T800H/3900-2.

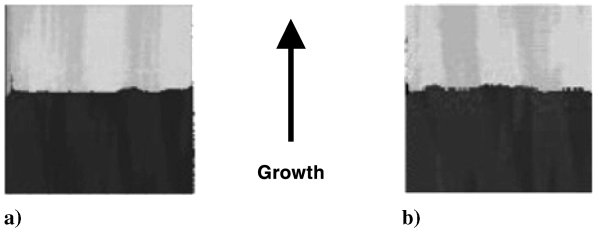

Fig. 14 Typical precrack shapes in T800H/3900-2: a) ENF; b) 4ENF.

this material, there is essentially no effect of Δa or specimen thickness on the precracked value of G_{IIc}^{max}. It is likely that this behavior can be traced to the fact that this material has a highly ductile interlaminar zone and exhibits predominately shear yielding behavior with only a small amount of damage [23,24]. Thus, considering the previous discussion on the way in which Δa affects toughness, for T800H there is little change in the near-tip zone with Δa, and it follows that there is also little effect of precrack length on G_{IIc}^{max}. Also note that in contrast to the IM7 results, the precracked value of G_{IIc}^{max} in Fig. 12 is generally larger than the nonprecracked value. Similar results for T800H/3900-2 have been reported in [11,23,24]. The reason this occurs in this and a few other materials [4,31] is not well understood, although it may well be related to the complex interaction of the initiation of mode-I microcracks that form into the mode-II crack for materials with highly ductile resins containing a blunt crack tip in a resin-rich region [23,31,32].

Considering the results for G_{IIc}^{NL} presented in Fig. 13, it may be observed that there once again is no effect of thickness or precracking method on G_{IIc}^{NL}. However, there may be some effect of Δa. In this figure, all points outside of the dotted ellipse were obtained from 4ENF tests or from ENF tests with large a/L that exhibited relatively slow crack advance. For these points, it is observed that G_{IIc}^{NL} is essentially independent of Δa. Conversely, all points within the dotted ellipse were obtained from ENF tests with $a/L \approx 0.6$ (cf. Table 1), which produced relatively dynamic crack advance. In general, these points appear to produce a larger G_{IIc}^{NL} than those outside of the ellipse. Thus, it is possible that the dynamically advanced cracks show delamination fronts that have slightly less near-tip damage. If this effect were small, then it would not be apparent in the C-scan images, and it would not make a significant difference in the value of G_{IIc}^{max}. However, lesser near-tip damage means less propagation of this damage at subcritical loads, and so the effect would be apparent at the nonlinear point. However, there is insufficient data for this to be more than conjecture at this point. What *is* clear from Figs. 12 and 13 is that any approach for creating long straight precracks that produce a minimum toughness in the IM7 material will also produce acceptable results for T800H.

Discussion

Considering that the goals of this study were to develop a method of precracking for potential use in an ASTM standardized ENF test,

any method that is chosen should produce toughness values that are accurate, reasonably conservative in comparison with those that would be observed in practical structural geometries, and repeatable. To obtain an accurate toughness, a precrack is required that 1) has a relatively straight delamination front, 2) is essentially perpendicular to the direction of crack advance, and 3) is representative of a naturally occurring delamination. These requirements will be satisfied by a straight precrack that is created by any of the methods studied. In view of the relationship between $G_{\mathrm{II}c}$ and Δa, the requirement of conservativeness will be satisfied by a method that can deliver relatively long straight precracks. The repeatability requirement implies that the precracking method that is chosen will consistently deliver precracks that fit the preceding criteria and that it is independent of the test operator and facility. It is this requirement that is perhaps the most difficult to achieve. This situation is exacerbated by the fact that the shape of a static mode-II precrack used in a mode-II test cannot be visually assessed after the test is completed. This has been reported in other studies [5,13,33] and was also verified in the present work. To complicate things further, as part of this study, the C-scan images were used to assess the accuracy by which visual measurements of crack length along the edge of the specimen could be made. Measurements were taken with and without magnification by two different test operators with the specimen under load as well as unloaded. These visual assessments were then compared with those obtained from the C-scans, from which it was concluded that visual assessments are accurate to only about 3 mm on either edge. This is greater than the criterion used for the difference in crack lengths ($a_{\max} - a_{\min}$) that defines whether a precrack is straight. Thus, because using a C-scan to verify delamination-front shapes in practice is impractical, it is apparent that any precracking method that is chosen must produce straight precracks without the need for visual corroboration.

Reviewing the IM7 results from this study, recall that all precracks created using I24-2 specimens with $2L = 88.9$ mm and $a/L = 0.6$ (geometry I24B) produced straight precracks, whereas all those created using specimens from the same plate with $2L = 114.3$ mm and $a/L = 0.5$ (geometry I24C) produced CWS precracks. For the former geometry, $L - a = 17.78$ mm, and for the latter, $L - a = 28.58$ mm. Also, precracking geometry I32B, with $L - a = 24.13$ mm, sometimes produced straight delamination fronts and sometimes produced CWS fronts. Thus, it was of interest to determine what would be obtained from specimens precracked in the ENF using a value of $L - a$ between 17.78 and 24.13 mm. To this end, [8] describes the results of a short follow-up study, in which the remaining I24-2 specimens were tested using $2L = 101.6$ mm and $a/L = 0.6$ ($L - a = 20.32$ mm). All specimens used in the present study and in the study of [8] were stored in desiccant from the time of manufacture until testing, and so there is no effect of moisture absorption from the environment on these data.

Figure 15 presents typical delamination-front shapes from the three different precracking geometries used on the I24-2 specimens. The top row of C-scan images presents results from the geometry with $L - a = 28.58$ mm. Here, all CWS fronts were obtained. The next row presents results from the new tests performed as part of the study of [8], where $L - a = 20.32$ mm. Of these, the second specimen from the left has $a_{\max} - a_{\min} = 3.3$ mm, and therefore fails our criterion for straightness, and the other three pass. However, in general, all four of these scans look relatively similar and represent a significant improvement from those shown in the first row. The final row of results in Fig. 15 are typical scans from those specimens tested with $L - a = 17.78$ mm, for which all delamination fronts pass the criterion for straightness. Visually, these delamination fronts also appear to be straighter than those in the previous row.

In view of the preceding, the recommendation from this study is that static mode-II precracking be performed using $a/L = 0.6$ and $2L = 86$–100 mm, with span lengths in the shorter end of the range being preferable. For the two materials studied in this work, this will produce precracks that are essentially straight and perpendicular to the direction of crack advance. It will also produce a sufficient amount of dynamic advance during precracking for the precracked toughness to be within the minimum-toughness regime. Further, in view of the studies on test geometries performed herein and in [8,18], the same geometry can be used for testing. This means that, if desired, nonprecracked and precracked toughnesses may be obtained from the same specimen.

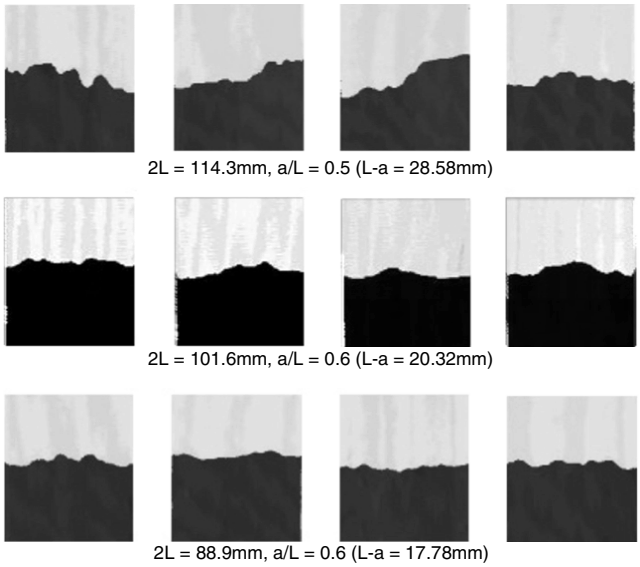

Fig. 15 ENF precrack shapes from follow-up study [8].

Conclusions

A study was conducted to evaluate and develop static mode-II precracking methods for use with the end-notched flexure test. As part of this study, 136 tests on two different materials were performed. This included specimens precracked using the 4ENF geometry and a large variety of different ENF geometries. It was concluded that there is no difference in the quality of precracks created by the ENF versus the 4ENF, and there is therefore no reason to use the more cumbersome procedure associated with 4ENF precracking and ENF testing. However, it was observed that there was a strong dependence of $G_{\mathrm{II}c}$ on the amount of dynamic crack advance that occurs during the precracking process. It was hypothesized that larger amounts of crack advance correspond to faster crack speeds and that the mechanisms associated with this effect are responsible for the observed behaviors. To address this, various precracking geometries were studied to determine those that would produce precracks that were essentially straight, perpendicular to the direction of crack advance, and of sufficient length to produce a precracked toughness that will be at or near the minimum value that occurs with increasing precrack length. This resulted in a recommended ENF precracking geometry that is also appropriate for testing, which allows for nonprecracked and precracked toughnesses to be obtained from the same test specimen.

Acknowledgments

This work was funded through the NASA Constellation University Institutes Project, NASA Cooperative Agreement NCC3-994, the "Institute for Future Space Transport."

References

[1] Davidson, B. D., and Sun, X., "Effects of Friction, Geometry and Fixture Compliance on the Perceived Toughness from Three and Four Point Bend End Notched Flexure Tests," *Journal of Reinforced Plastics and Composites*, Vol. 24, No. 15, 2005, pp. 1611–1628. doi:10.1177/0731684405050402

[2] Sun, X., and Davidson, B. D., "Numerical Evaluation of the Effects of Friction and Geometrical Nonlinearities on Three and Four Point Bend End Notched Flexure Test Results," *Engineering Fracture Mechanics*, Vol. 73, No. 10, 2006, pp. 1343–1361. doi:10.1016/j.engfracmech.2005.11.007

[3] Davidson, B. D., Sun, X., and Vinciquerra, A. J., "Influences of Friction, Geometric Nonlinearity and Fixture Compliance on Three and Four Point Bend End Notched Flexure Test Results," *Journal of Composite Materials*, Vol. 41, No. 10, 2007, pp. 1177-1196. doi:10.1177/0021998306067304

[4] Murri, G. B., and Martin, R. H., "Effect of Initial Delamination on Mode I and Mode II Interlaminar Fracture Toughness and Fatigue Fracture Threshold," *Composite Materials: Fatigue and Fracture*, Vol. 4, ASTM STP 1156, edited by W. W. Stinchcomb and N. E. Ashbaugh, American Society for Testing and Materials, Philadelphia, 1993, pp. 239–256.

[5] O'Brien, T. K., Murri, G. B., and Salpekar, S. A., "Interlaminar Shear Fracture Toughness and Fatigue Thresholds for Composite Materials," *Composite Materials: Fatigue and Fracture*, Vol. 2, ASTM STP 1012, edited by P. A. Lagace, American Society for Testing and Materials, Philadelphia, 1989, pp. 222–250.

[6] Russell, A. J., "Initiation and Growth of Mode II Delamination in Toughened Composites," *Composite Materials: Fatigue and Fracture*, Vol. 3, ASTM STP 1110, edited by T. K. O'Brien, American Society for Testing and Materials, Philadelphia, 1991, pp. 226–242.

[7] Davidson, B. D., and Koudela, K. L., "Influence of the Mode Mix of Precracking on the Delamination Toughness of Laminated Composites," *Journal of Reinforced Plastics and Composites*, Vol. 18, No. 15, 1999, pp. 1408–1414.

[8] Davidson, B. D., "Towards an ASTM Standardized Test for Determining G_{IIc} of Unidirectional Laminated Polymeric Matrix Composites," *Proceedings of the American Society for Composites: 21st Technical Conference* [CD-ROM], DEStech Publications, Lancaster, PA, Sept. 2006.

[9] Martin, R. H., and Davidson, B. D., "Mode II Fracture Toughness Evaluation Using a Four Point Bend End-Notched Flexure Test," *Plastics, Rubber and Composites Processing and Applications*, Vol. 28, No. 8, 1999, pp. 401–406.

[10] Schuecker, C., and Davidson, B. D., "Evaluation of the Accuracy of the Four-Point Bend End-Notched Flexure Test for Mode II Delamination Toughness Determination," *Composites Science and Technology*, Vol. 60, No. 11, 2000, pp. 2137–2146. doi:10.1016/S0266-3538(00)00113-5

[11] Vinciquerra, A. J., and Davidson, B. D., "Effect of Crack Length Measurement Technique and Data Reduction Procedures on the Perceived Toughness from Four-Point Bend End-Notched Flexure Tests," *Journal of Reinforced Plastics and Composites*, Vol. 23, No. 10, 2004, pp. 1051–1062. doi:10.1177/0731684404035413

[12] Polaha, J. J., Davidson, B. D., Hudson, R. C., and Pieracci, A., "Effects of Mode Ratio, Ply Orientation and Precracking on the Delamination Toughness of a Laminated Composite," *Journal of Reinforced Plastics and Composites*, Vol. 15, No. 2, 1996, pp. 141–173.

[13] Carlsson, L. A., Gillespie, J. W., and Trethewey, B. R., "Mode II Interlaminar Fracture of Graphite/Epoxy and Graphite/PEEK," *Journal of Reinforced Plastics and Composites*, Vol. 5, No. 3, 1986, pp. 170–187. doi:10.1177/073168448600500302

[14] Davies, P., Ducept, F., Brunner, A. J., Blackman, B. R. K., and de Morais, A. B., "Development of a Standard Mode II Shear Fracture Test Procedure," *ECCM7: Seventh European Conference on Composite Materials*, Vol. 2, Woodhead Publishing, Cambridge, England, U.K., May 1996, pp. 9–15.

[15] Odagiri, N., Kishi, H., and Yamashita, M., "Development of TORAYCA Prepreg P2302 Carbon Fiber Reinforced Plastic for Aircraft Primary Structural Materials," *Advanced Composite Materials*, Vol. 5, No. 3, 1996, pp. 249–254.

[16] Davidson, B. D., Gharibian, S. J., and Yu, L., "Evaluation of Energy Release Rate-Based Approaches for Predicting Delamination Growth in Laminated Composites," *International Journal of Fracture*, Vol. 105, No. 4, 2000, pp. 343–365. doi:10.1023/A:1007647226760

[17] Davidson, B. D., Bialaszewski, R. D., and Sainath, S. S., "A Non-Classical, Energy Release Rate Based Approach for Predicting Delamination Growth in Graphite Reinforced Laminated Polymeric Composites," *Composites Science and Technology*, Vol. 66, No. 10, 2006, pp. 1479–1496. doi:10.1016/j.compscitech.2004.10.031

[18] Davidson, B. D., and Sun, X., "Geometry and Data Reduction Recommendations for a Standardized End Notched Flexure Test for Unidirectional Composites," *Journal of ASTM International*, Vol. 3, No. 9, 2006, Paper JAI10028510.1520/JAI100285.

[19] Davidson, B. D., Altonen, C. S., and Polaha, J. J., "Effect of Stacking Sequence on Delamination Toughness and Delamination Growth Behavior in Composite End-Notched Flexure Specimens," *Composite Materials: Testing and Design*, Vol. 12, ASTM STP 1274, edited by R. B. Deo and C. R. Saff, American Society for Testing and Materials, Philadelphia, 1996, pp. 393–413.

[20] Davidson, B. D., Yu, L., Lundberg, S. D., and Rao, L. M., "Accuracy Assessment of a Three-Dimensional, Crack Tip Element Based Approach for Predicting Delamination Growth in Stiffened-Skin Geometries," *International Journal of Fracture*, Vol. 132, No. 1, 2005, pp. 1–32. doi:10.1007/s10704-004-8155-y

[21] Davidson, B. D., Michaels, J. E., Sundararaman, V., and Michaels, T. E., "Ultrasonic Imaging of Impact Damaged Composite Panels," *Acoustical Imaging*, edited by H. Ermert and H.-P. Harjes, Vol. 19, Plenum, New York, 1992, pp. 589–594.

[22] Vinciquerra, A. J., Davidson, B. D., Schaff, J. R., and Smith, S. L., "An Improved Methodology for the Determination of Mode II Fatigue Delamination Growth Rates Using the End-Notched Flexure Test," *Proceedings of the 15th Annual American Society for Composites Technical Conference*, edited by O. O. Ochoa, T. K. O'Brien, D. Lagoudas and H. J. Sue, Technomic Publishing, Lancaster, PA, 2000, pp. 999–1007.

[23] Matsuda, S., Hojo, M., and Ochiai, S., "Mesoscopic Fracture Mechanism of Mode II Delamination Fatigue Crack Propagation in Interlayer-Toughened CFRP," *JSME International Journal, Series A (Mechanics and Material Engineering)*, Vol. 40, No. 4, 1997, pp. 423–429.

[24] Kageyama, K., Kimpara, I., Ohsawa, I., Hojo, N., and Kabashima, S., "Mode I and Mode II Delamination Growth of Interlayer Toughened Carbon/Epoxy (T800H/3900-2) Composite System," *Composite Materials: Fatigue and Fracture*, Vol. 5, ASTM STP 1230, edited by R. H. Martin, American Society for Testing and Materials, Philadelphia, 1995, pp. 19–37.

[25] Neal, D., and Vangel, M., "Statistical Analysis of Mechanical Properties," *Engineered Materials Handbook*, Vol. 1, ASM International, Metals Park, OH, 1987, pp. 302–307.

[26] Davidson, B. D., Krüger, R., and König, M., "Three Dimensional Analysis and Resulting Design Recommendations for Unidirectional and Multidirectional End-Notched Flexure Tests," *Journal of Composite Materials*, Vol. 29, No. 16, 1995, pp. 2108–2133.

[27] Kinloch, A. J., and Young, R. J., *Fracture Behaviour of Polymers*, Elsevier Applied Science, London, 1983.

[28] Fracasso, R., Rink, M., Pavan, A., and Frassine, R., "The Effects of Strain-Rate and Temperature on the Interlaminar Fracture Toughness of Interleaved PEEK/CF Composites," *Composites Science and Technology*, Vol. 61, No. 1, 2001, pp. 57–63. doi:10.1016/S0266-3538(00)00153-6

[29] Lim, W. W., and Mizumachi, H., "Fracture Toughness of Adhesive Joints, 3: Temperature and Rate Dependencies of Mode II Fracture Toughness and Adhesive Shear Strength," *Journal of Applied Polymer Science*, Vol. 63, No. 7, 1997, pp. 835–841. doi:10.1002/(SICI)1097-4628(19970214)63:7<835::AID-APP2>3.0.-CO;2-R

[30] Tsai, J. L., Guo, C., and Sun, C. T., "Dynamic Delamination Fracture Toughness in Unidirectional Polymeric Composites," *Composites Science and Technology*, Vol. 61, No. 1, 2001, pp. 87–94. doi:10.1016/S0266-3538(00)00197-4

[31] O'Brien, T. K., "Composite Interlaminar Fracture Toughness, G_{IIc}: Shear Measurement or Sheer Myth?," *Composite Materials: Fatigue and Fracture*, Vol. 7, ASTM STP 1330, edited by R. B. Bucinell, American Society for Testing and Materials, Philadelphia, 1998, pp. 3–18.

[32] Lee, S. M., "Mode II Interlaminar Crack Growth Process in Polymer Matrix Composites," *Journal of Reinforced Plastics and Composites*, Vol. 18, No. 13, 1999, pp. 1254–1266.

[33] Davies, P., Kausch, H. H., Williams, J. G., Kinloch, A. J., Charalambides, M. N., Pavan, A., Moore, D. R., Prediger, R., Robinson, I., Burgoyne, N., Friedrich, K., Wittich, H., Rebelo, C. A., Torres Marques, A., Ramsteiner, F., Melve, B., Fischer, M., Roux, N., Martin, D., Czarnocki, P., Neville, D., Verpoest, I., Goffaux, B., Lee, R., Walls, K., Trigwell, N., Partridge, I. K., Jaussaud, J., Andersen, S., Giraud, Y., Hale, G., and McGrath, G., "Round-Robin Interlaminar Fracture Testing of Carbon-Fibre-Reinforced Epoxy and PEEK Composite," *Composites Science and Technology*, Vol. 43, No. 2, 1992, pp. 129–136. doi:10.1016/0266-3538(92)90003-L

K. Shivakumar
Associate Editor